Research Article | Vol. 25, No. 25 | 11 Dec 2017 | OPTICS EXPRESS 30820
Optics EXPRESS

Tunable third harmonic generation of vortex beams in an optical superlattice

YU WU,[1] RUI NI,[1] ZHOU XU,[1] YAODONG WU,[1] XINYUAN FANG,[1] DAN WEI,[1] XIAOPENG HU,[1,*] YONG ZHANG,[1] MIN XIAO,[1,2] AND SHINING ZHU[1]

[1]*National Laboratory of Solid State Microstructure, College of Engineering and Applied Sciences and School of Physics, Nanjing University, Nanjing 210093, China*
[2]*Department of Physics, University of Arkansas, Fayetteville, Arkansas 72701, USA*
**xphu@nju.edu.cn*

Abstract: We report generation of tunable vortex beams in the blue spectral range, with a 3.3 nm spectral tuning range, by frequency tripling of the near-infrared (IR) wave at around 1.34 um in a $LiTaO_3$ optical superlattice. The nonlinear crystal used in this work has a chirped dual-periodical structure which can provide two expanded reciprocal vectors for tunable performance of the cascaded third harmonic generation (THG). The maximum THG efficiency reaches about 1.4%.

OCIS codes: (080.4865) Optical vortices; (190.2620) Harmonic generation and mixing; (140.3600) Lasers, tunable.

References and links

1. L. Allen, M. W. Beijersbergen, R. J. C. Spreeuw, and J. P. Woerdman, "Orbital angular momentum of light and the transformation of Laguerre-Gaussian laser modes," Phys. Rev. A **45**(11), 8185–8189 (1992).
2. S. W. Hell, "Toward fluorescence nanoscopy," Nat. Biotechnol. **21**(11), 1347–1355 (2003).
3. D. G. Grier, "A revolution in optical manipulation," Nature **424**(6950), 810–816 (2003).
4. A. Mair, A. Vaziri, G. Weihs, and A. Zeilinger, "Entanglement of the orbital angular momentum states of photons," Nature **412**(6844), 313–316 (2001).
5. D. S. Ding, Z. Y. Zhou, B. S. Shi, and G. C. Guo, "Single-photon-level quantum image memory based on cold atomic ensembles," Nat. Commun. **4**, 2527 (2013).
6. E. Nagali, F. Sciarrino, F. De Martini, L. Marrucci, B. Piccirillo, E. Karimi, and E. Santamato, "Quantum information transfer from spin to orbital angular momentum of photons," Phys. Rev. Lett. **103**(1), 013601 (2009).
7. A. E. Willner, H. Huang, Y. Yan, Y. Ren, N. Ahmed, G. Xie, C. Bao, L. Li, Y. Cao, Z. Zhao, J. Wang, M. P. J. Lavery, M. Tur, S. Ramachandran, A. F. Molisch, N. Ashrafi, and S. Ashrafi, "Optical communications using orbital angular momentum beams," Adv. Opt. Photonics **7**(1), 66–106 (2015).
8. M. W. Beijersbergen, R. P. C. Coerwinkel, M. Kristensen, and J. P. Woerdman, "Helical-wavefront laser beams produced with a spiral phase plate," Opt. Commun. **112**(5–6), 321–327 (1994).
9. N. R. Heckenberg, R. McDuff, C. P. Smith, and A. G. White, "Generation of optical phase singularities by computer-generated holograms," Opt. Lett. **17**(3), 221–223 (1992).
10. D. Naidoo, F. S. Roux, A. Dudley, I. Litvin, B. Piccirillo, L. Marrucci, and A. Forbes, "Controlled generation of higher-order Poincaré sphere beams from a laser," Nat. Photonics **10**, 327–332 (2016).
11. A. Forbes, "Controlling light's helicity at the source: orbital angular momentum states from lasers," Philos Trans A Math Phys Eng Sci **375**(2087), 20150436 (2017).
12. W. Ji, C.-H. Lee, P. Chen, W. Hu, Y. Ming, L. Zhang, T.-H. Lin, V. Chigrinov, and Y.-Q. Lu, "Meta-q-plate for complex beam shaping," Sci. Rep. **6**, 25528 (2016).
13. G. Li, M. Kang, S. Chen, S. Zhang, E. Y. Pun, K. W. Cheah, and J. Li, "Spin-Enabled Plasmonic Metasurfaces for Manipulating Orbital Angular Momentum of Light," Nano Lett. **13**(9), 4148–4151 (2013).
14. X. Cai, J. Wang, M. J. Strain, B. Johnson-Morris, J. Zhu, M. Sorel, J. L. O'Brien, M. G. Thompson, and S. Yu, "Integrated compact Optical Vortex Beam Emitters," Science **338**(6105), 363–366 (2012).
15. P. Miao, Z. Zhang, J. Sun, W. Walasik, S. Longhi, N. M. Litchinitser, and L. Feng, "Orbital angular momentum microlaser," Science **353**(6298), 464–467 (2016).
16. N. Apurv Chaitanya, S. Chaitanya Kumar, K. Devi, G. K. Samanta, and M. Ebrahim-Zadeh, "Ultrafast optical vortex beam generation in the ultraviolet," Opt. Lett. **41**(12), 2715–2718 (2016).
17. X. Fang, G. Yang, D. Wei, D. Wei, R. Ni, W. Ji, Y. Zhang, X. Hu, W. Hu, Y. Q. Lu, S. N. Zhu, and M. Xiao, "Coupled orbital angular momentum conversions in a quasi-periodically poled $LiTaO_3$ crystal," Opt. Lett. **41**(6), 1169–1172 (2016).
18. J. Yang, X. P. Hu, P. Xu, X. J. Lv, C. Zhang, G. Zhao, H. J. Zhou, and S. N. Zhu, "Chirped-quasi-periodic structure for quasi-phase-matching," Opt. Express **18**(14), 14717–14723 (2010).

#308410 https://doi.org/10.1364/OE.25.030820
Journal © 2017 Received 2 Oct 2017; revised 15 Nov 2017; accepted 21 Nov 2017; published 27 Nov 2017

Optics EXPRESS

19. B. Q. Chen, M. L. Ren, R. J. Liu, C. Zhang, Y. Sheng, B. Q. Ma, and Z. Y. Li, "Simultaneous broadband generation of second and third harmonics from chirped nonlinear photonic crystals," Light Sci. Appl. **3**, e189 (2014).
20. Z. W. Liu, S. N. Zhu, Y. Y. Zhu, Y. Q. Qin, J. L. He, C. Zhang, H. T. Wang, N. B. Ming, X. Y. Liang, and Z. Y. Xu, "Quasi-CW ultraviolet generation in a dual-periodic LiTaO3 superlattice by frequency tripling," Jpn. J. Appl. Phys. **40**, 6841–6844 (2001).
21. S. N. Zhu, Y. Y. Zhu, Z. Y. Zhang, H. Shu, H. F. Wang, J. F. Hong, C. Z. Ge, and N. B. Ming, "$LiTaO_3$ crystal periodically poled by applying an external pulsed field," J. Appl. Phys. **77**(10), 5481–5483 (1995).
22. G. H. Shao, Z. J. Wu, J. H. Chen, F. Xu, and Y. Q. Lu, "Nonlinear frequency conversion of fields with orbital angular momentum using quasi-phase-matching," Phys. Rev. A **88**(6), 063827 (2013).
23. X. P. Hu, P. Xu, and S. N. Zhu, "Engineered quasi-phase-matching for laser techniques," Photonics Res. **1**(4), 171–185 (2013).

1. Introduction

Vortex beams refer to light field with a "twisted" or helical phase structure of the form $\exp(il\theta)$ and possesses a phase singularity in the beam center, where l refers to the topological charge and θ is the azimuthal angle. Vortex beams carry nonzero orbital angular momentum (OAM), whose value equals to $l\hbar$. Vortex beam was first raised by Allen in 1992 [1], and has many applications in optical microscopic [2], micromanipulation [3], quantum information processing [4–6], large-capacity optical telecommunication [7]. To produce such vortex beams, several methods can be used, such as spiral phase plate [8], holographic diffracting optical elements [9], manipulation of modes in laser cavities [10,11],liquid crystal *q*-plate and meta-*q*-plate exploiting geometric phase [12,13]. Recently, integrated on-chip laser light sources carrying OAM have been developed for compact solutions [14,15]. Besides, second-order nonlinear frequency conversion has been proved to be a promising alternative for generating vortex beams at new frequencies with conserved topological charges. For frequency up-conversions, intense vortex beams in the blue to ultraviolet spectral range, were obtained through second harmonic generation (SHG) [16] or cascaded THG [17]. However, the operating wavelength of such method has limited tuning range due to the phase-matching characteristics of frequency up-conversions. To control the wavelength acceptance bandwidth of cascaded nonlinear optical processes, chirped quasi-periodical [18] and chirped dual-periodical optical superlattice [19] were proposed, and broadband THG was experimentally demonstrated with a Gaussian-profiled pumping wave.

In this paper, we use a chirped dual-periodical optical superlattice as the nonlinear crystal, in which THG is realized through SHG of the fundamental wave (FW) cascading sum frequency generation (SFG) of the FW and the generated second harmonic (SH) waves. By proper design of the two reciprocal vectors used for the coupled two nonlinear processes, blue lights with 3.3-nm spectral tuning range are obtained with moderate efficiency, and the topological charge of the generated third harmonic (TH) wave is three times which imprinted on the FW.

2. Design of the optical superlattice

A dual-periodical structure can be looked upon as periodic phase-reversal sequence superimposed on another periodic structure and the reciprocal vectors provided by the dual-periodic optical superlattice can be expressed as [20]:

$$G_{m,n} = G_m + G_n = \frac{2\pi m}{\Lambda_1} + \frac{2\pi n}{\Lambda_2}. \quad (1)$$

Where Λ_1 and Λ_2 are the periods of the periodic structure and the modulating structure respectively. The integers *m* and *n* indicate the order of the reciprocal vectors.

The Fourier coefficients of the structure are:

Optics EXPRESS

$$f_{m,n} = f_m f_n = \frac{4}{mn\pi^2}\sin(mD_1\pi)\sin(nD_2\pi) \tag{2}$$

Where D_1 and D_2 are the duty cycles of the two modulating periods.

We chose congruent $LiTaO_3$ (CLT) as the nonlinear crystal. The starting wavelength of the FW was chosen to be 1342 nm and the working temperature was set to be 150 °C. Considering the difficulty in poling domain periods of several microns, we chose two higher order reciprocal vectors $G_{3,-1}$ and $G_{3,1}$, as indicated in Fig. 1, to compensate for the wave-vector mismatches in the SHG and SFG processes, and the lengths of the two modulating periods were calculated to be $\Lambda_1 = 21.7\mu m$ and $\Lambda_2 = 14.4\mu m$ respectively.

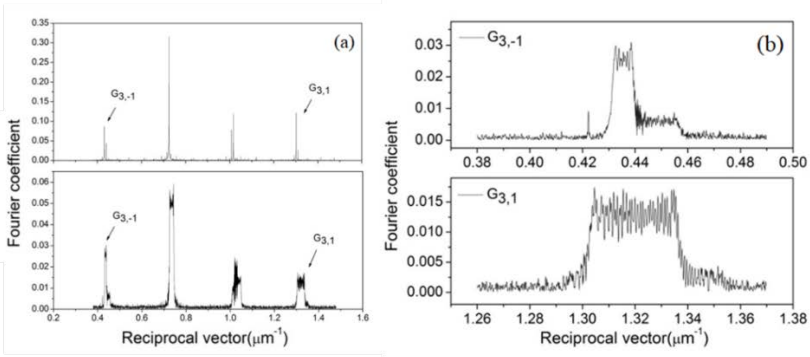

Fig. 1. (a) The Fourier spectrum of the dual-periodical poled LT and the chirped dual-periodical poled LT, (b) Detailed Fourier spectrum of the reciprocal vectors $G_{3,-1}$ and $G_{3,1}$ of the chirped dual-periodical structure.

A chirped periodical structure refers to the structure where the periods of the domain vary slightly at different position along the direction of propagation, and the bandwidth of the reciprocal vectors provided by the chirped periodical structure will be expanded. Thus, the acceptance bandwidth of quasi-phase-matched nonlinear processes in this structure will be expanded.

By introducing chirp into dual-periodical structure, the two reciprocal vectors used for THG can be expanded as:

$$\begin{cases} G_{3,-1}(x) = 3\times\dfrac{2\pi}{\Lambda_1} - \dfrac{2\pi}{\Lambda_2} + \varphi_1\dfrac{x}{L/2} = 3\times\dfrac{2\pi}{\Lambda_1(x)} - \dfrac{2\pi}{\Lambda_2(x)} \\ G_{3,1}(x) = 3\times\dfrac{2\pi}{\Lambda_1} - \dfrac{2\pi}{\Lambda_2} - \varphi_2\dfrac{x}{L/2} = 3\times\dfrac{2\pi}{\Lambda_1(x)} + \dfrac{2\pi}{\Lambda_2(x)} \end{cases}. \tag{3}$$

Where L is the total length of the structure, $\Lambda_1(x)$ and $\Lambda_2(x)$ are the two modulating periods after chirp has been introduced into the structure. φ_1 and φ_2 characterize the range of wave-vector mismatch in the expanded SHG and SFG processes. Here, in order to tune the input wavelength within a range of about 10 nm, we set

$$\varphi_1 = \Delta k_1(1332nm) - \Delta k_1(1342nm) = 1969.2m^{-1}$$
$$\varphi_2 = \Delta k_2(1332nm) - \Delta k_2(1342nm) = 8859.3m^{-1}.$$

Optics EXPRESS

Where $\Delta k_1(\lambda)$ and $\Delta k_2(\lambda)$ are the wave-vector mismatch for the SHG and SFG process respectively, and λ is the wavelength of the FW. The two modulating periods of the chirped dual-periodical structure can be derived from Eq. (3) as:

$$\begin{cases} \Lambda_1(x) = \dfrac{1}{\dfrac{1}{\Lambda_1} + (\varphi_1 + \varphi_2)\dfrac{x}{6L\pi}} \\ \Lambda_2(x) = \dfrac{1}{\dfrac{1}{\Lambda_2} + (\varphi_1 - \varphi_2)\dfrac{x}{2L\pi}} \end{cases}. \tag{4}$$

The Fourier spectrum of the chirped dual-periodical structure is shown in Fig. 1(b), and one can see that the two reciprocal vectors $G_{3,-1}$ and $G_{3,1}$ are expanded compared with that of the dual-periodical structure in Fig. 1(a). What one should note is that there is a jump in the spectrum of $G_{3,-1}$. This is the result of overlapping between the two adjacent reciprocal vectors which are very close to each other, and the detail can be found in the upper part of Fig. 1(a). Actually, only the higher flat part of the expanded reciprocal vector $G_{3,-1}$ was used in the experiment.

3. Results and discussions

The optical superlattice with a thickness of 0.5 mm was fabricated using the electric field poling technique at room temperature [21], and the length of the sample was 20 mm. Figure 2 shows the microphotograph of the etched surface of the sample.

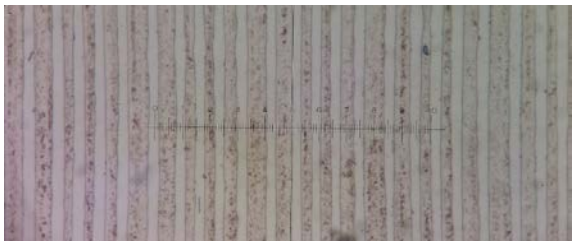

Fig. 2. Microphotograph of the chirped dual-periodical optical superlattice revealed by etching.

The sketch of the experimental setup is depicted in Fig. 3. The input FW with a spectral linewidth around 1nm is obtained from an optical parametric oscillator (Horizon I-8572, Continuum Co.) pumped by a nanosecond laser system with a pulse width of about 6 ns and a repetition rate of 10 Hz. The FW was shaped with a pinhole and was reflected by a phase-only spatial light modulator (Holoeye, GAEA-TELCO-033), then the Gaussian beam was converted into a vortex beam with topological charge l = 1.The power of the FW with a ring-shaped profile was 13 mW, and the polarization of the FW was parallel to the z-axis of the optical superlattice to make use of the largest nonlinear coefficient d_{33}. A lens with a focusing length of 100 mm was used to focus the FW into the nonlinear crystal and the power intensity inside the crystal was estimated to be about 150 MW/cm^2. The crystal was embedded into a temperature-controlled oven and the temperature of the optical superlattice was kept at 150 °C. Two filters, Filter 1 and Filter 2 were used to filter the FW and the harmonic wave (SH/TH) respectively. The beam profile of the generated SH and TH waves were monitored with a CCD camera.

Optics EXPRESS

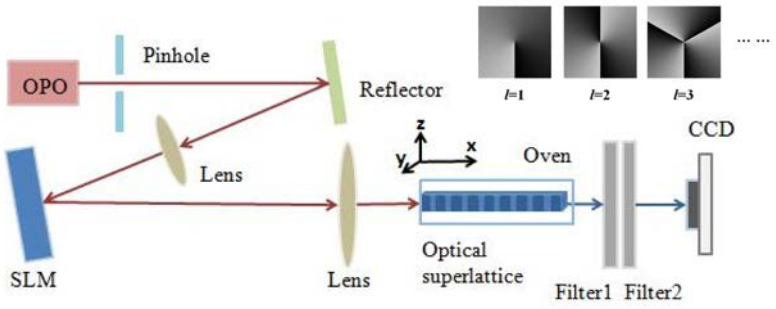

Fig. 3. Sketch of the experimental setup and the inset on the top right shows the helical phase profiles loaded on the SLM to generate the vortices.

By changing the wavelength of the FW, we experimentally investigated tunable THG in the chirped dual-periodical optical superlattice. Figure 4(a) gives the conversion efficiency of both the SH and TH waves when the wavelength of the FW was changed around 1.34 um with the topological charge of 1. From the figure we can see, when l = 1, the efficiency for SHG kept at around 7.5% with an acceptance bandwidth of about 10 nm (1335-1345 nm) as expected. The generated TH has a 3.3-nm spectral tuning range with the highest efficiency of around 1.4%.

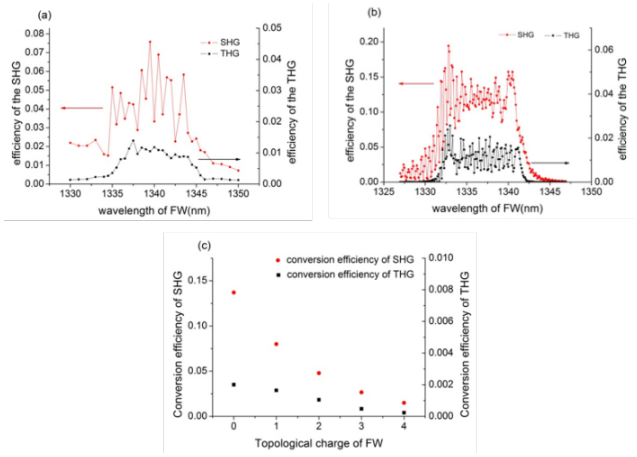

Fig. 4. (a) Measured and (b) Theoretical conversion efficiency of the SHG and THG processes depending on the wavelength of the FW with the topological charge of 1. (c) The measured conversion efficiency of SHG and THG processes depending on the FW with different topological charges.

For comparison, the theoretical acceptance bandwidths and conversion efficiencies of the SHG and THG processes in the chirped dual-periodical optical superlattice can be obtained by numerically solving the nonlinear coupled wave equations [22]:

$$\begin{cases} \dfrac{dE_1}{dx} = 2i\dfrac{\omega_1}{n_1 c} f(x) d_{eff} (E_2 E_1^* e^{-i\Delta k_1 x} + E_3 E_2^* e^{-i\Delta k_2 x}) \\ \dfrac{dE_2}{dx} = 2i\dfrac{\omega_2}{n_2 c} f(x) d_{eff} (\dfrac{1}{2} E_1^2 e^{i\Delta k_1 x} + E_3 E_1^* e^{-i\Delta k_2 x}) \\ \dfrac{dE_3}{dx} = 2i\dfrac{\omega_3}{n_3 c} f(x) d_{eff} E_1 E_2 e^{i\Delta k_2 x} \end{cases} . \quad (5)$$

Optics EXPRESS

The input wave is z-polarized and propagates along the x-axis of the nonlinear crystal. $E_i(r,x) = A_i(x)u_i(r,x)e^{il\varphi}e^{ik_i x}, (i=1,2,3)$ is the transverse electrical field of the FW, SH and TH waves, where $A_i(x)$ is the field amplitude, $u_i(r,x)$ is the transverse optical field distribution, l is the topological charge, and k_i is the wave vector. $\Delta k_1 = 2k_1 - k_2$ and $\Delta k_2 = k_1 + k_2 - k_3$ represent the phase mismatches of the SHG and THG respectively. $f(x)$ is the structure function, which only takes + 1 or –1, representing two inverse polarization directions in ferroelectric. In the chirped dual-periodical structure, the structure function is defined as:

$$\begin{cases} f(x) = +1, (x - \frac{\Lambda_1(x)}{2})(x - \frac{\Lambda_2(x)}{2}) > 0 \\ f(x) = -1, (x - \frac{\Lambda_1(x)}{2})(x - \frac{\Lambda_2(x)}{2}) < 0 \end{cases}. \quad (6)$$

By numerically solving the coupled wave equations with the parameters of the chirped dual-periodical structure used in our experiment, we plotted the theoretical curves for the conversion efficiencies of both the SH and TH processes in Fig. 4(b). The numerical result is consistent with the experimental one. We also measured the conversion efficiency of SHG and THG processes with respect to the topological charge of the FW, and Fig. 4(c) clearly shows that, the conversion efficiencies decrease with the increasing of the topological charge, which results from smaller overlapping integrals between the FW and the harmonic waves at higher topological charges.

The intensity profiles of the generated SH and TH waves recorded on the CCD camera are shown in Fig. 5. From the figure we can see that the harmonic waves maintain donut-shaped intensity profiles when the wavelength of the FW was tuned from 1335 nm to 1345 nm with a 2-nm step size. The topological charge imprinted on the FW was l = 1, and to reveal the topological charges of the generated harmonic waves, the SH and TH were converted to Hermite–Gaussian modes using a cylindrical lens. By counting the dark stripes shown in Fig. 4, the topological charge of SH and TH pattern were determined to be l = 2 and l = 3 with input topological charge of 1, which confirms the topological charge conservation law during nonlinear frequency conversions.

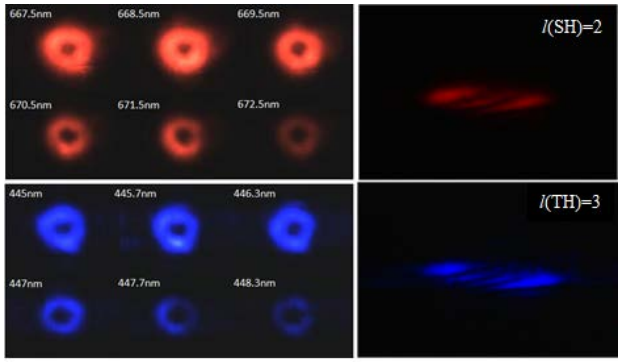

Fig. 5. The intensity profiles of the SH and TH waves, and the converted pattern after using a cylindrical lens, which indicates l = 2 for the SH wave and l = 3 for the TH wave.

We have also designed and fabricated another dual-periodical optical superlattice with a 20-nm acceptance bandwidth. However, with a same crystal length, the broader acceptance bandwidth will lead to lower nonlinear conversion efficiencies. The measured conversion efficiency was lower comparing with the one having a 10-nm acceptance bandwidth, which

Optics EXPRESS

was 5.7% for the SHG and 0.72% for the THG. To improve the nonlinear conversion efficiency, intense laser light sources carrying OAM with high beam quality are desirable.

4. Conclusions

We obtained tunable vortex beams in the blue through THG with a special designed domain-inverted $LiTaO_3$ crystal. The FW was in the near-IR at about 1.34 um and was imprinted with a topological charge of *l*. To achieve tunable THG, an optical superlattice with a chirped dual-periodical structure was used. The two expanded reciprocal vectors, $G_{3,-1}$ and $G_{3,1}$ can compensate for the wave-vector mismatches of the cascaded SHG and SFG processes. The acceptance bandwidth of the cascaded second-order nonlinear processes was measured to be 10 nm with a 7.5% conversion efficiency for the SHG and 1.4% for THG. In addition, the topological charges of the generated TH waves were measured to be 3 times that of the FW, which proved that OAM was conserved during THG. The wavelength of the generated blue light in this work is around 440 nm, which lies in the operating wavelength range of the commercial SLMs. To further obtain vortex light sources with shorter wavelengths (down to ultraviolet or vacuum ultraviolet), which are not supported by the commercial SLMs, one can change the nonlinear crystals from congruent $LiTaO_3$/$LiNbO_3$ to stoichiometric ones, or to crystal quartz or $BaMgF_4$ with a proper designed quasi-phase-matching structure [23].

Funding

National Key R&D Program of China (2017YFA0303700); National Natural Science Foundation of China (NSFC) (11674171, 91636106, 11627810 and J1310026); Jiangsu Science Foundation (BK20151374); PAPD of Jiangsu Higher Education Institutions.